

1 **Comparative analysis of network-based measures for the**
2 **assessment of drug-induced liver injury: A case study of**
3 ***Hypericum perforatum***

4 Anonymous Author(s)

Author information removed for double-blind review

5 **Abstract**

6 Network-based metrics are widely used to identify associations between compounds and diseases, as-
7 suming that proximity within a protein–protein interaction network reflects functional relevance. How-
8 ever, these metrics are often reported as Z-scores, which we demonstrate are fundamentally sensitive to
9 the number of targets a compound possesses. This dependency introduces a systematic bias where com-
10 pounds with broad polypharmacology appear statistically significant due to null distribution tightening
11 (the Law of Large Numbers) rather than physical network reachability.

12 Here, we systematically evaluate this bias using the human liver interactome and a controlled com-
13 parison of two constituents from *Hypericum perforatum*. We show that conventional proximity Z-scores
14 yield unstable rankings that reverse depending on network construction parameters. While a compound
15 with many targets may achieve a higher Z-score, it can remain physically more distant from the dis-
16 ease module than a compound with fewer, high-leverage targets. We resolve this by utilizing random
17 walk–based influence propagation and introducing a size-normalized metric: perturbation efficiency.
18 Our results show that influence-base rankings are stable across varied network thresholds and correctly
19 identify high-leverage modulators that proximity metrics miss. This study provides a methodological
20 template for identifying and correcting statistical artifacts in network medicine, enabling more reliable
21 risk assessment in complex biological systems.

22 **Keywords:** network propagation, proximity metrics, metric robustness, drug-induced liver injury, polyphar-
23 macology, Z-score confounding, perturbation efficiency.

24 1 Introduction

25 Network-based prioritization is a cornerstone of modern systems biology and drug discovery, assuming
26 that the topological proximity between compound targets and disease genes within a protein–protein
27 interaction (PPI) network reflects functional relevance [Hopkins, 2008, Barabási et al., 2011, Guney
28 et al., 2016, Menche et al., 2015]. Because raw network distances are sensitive to local topology and
29 degree distribution, they are typically reported as Z-scores relative to degree-matched null models. While
30 these Z-scores are intended to quantify statistical significance, they are fundamentally confounded by the
31 number of targets a compound possesses. As the number of seed nodes increases, the variance of the
32 null distribution decreases (the Law of Large Numbers), leading to deterministic significance inflation
33 for compounds with broad polypharmacology. Identifying whether such results reflect true biological
34 influence, or whether they represent systematic artifacts of distance-based inference, is essential for the
35 reliability of network medicine.

36 Using the human liver interactome as a model system, we investigate this confounding effect through
37 a controlled comparison of two constituents from *Hypericum perforatum* (St. John’s Wort). These con-
38 stituents—Hyperforin and Quercetin—exhibit highly asymmetric target set sizes: Hyperforin possesses
39 10 validated targets, while Quercetin has over 60 [Nahrstedt and Butterweck, 1997, Moore et al., 2000,
40 Boots et al., 2008]. This asymmetry provides a sharp stress test for network metrics. Conventional prox-
41 imity Z-scores predict greater disease-associated significance for the broad-spectrum modulator, even
42 when it is physically more distant from the disease module than the high-leverage modulator. This rever-
43 sal indicates that proximity-based prioritization is unstable across network construction parameters and
44 susceptible to sample-size artifacts.

45 Here, we evaluate the robustness of proximity-based and influence-based metrics for comparative
46 prioritization. We demonstrate that proximity Z-scores yield unstable, threshold-dependent rankings
47 driven by null-distribution tightening rather than physical reachability. To resolve this instability, we
48 utilize random walk–based influence propagation, which integrates over the entire network topology and
49 captures signal amplification through regulatory hubs [Köhler et al., 2008]. We introduce a normalized
50 metric, perturbation efficiency, to account for target set size and ensure unbiased comparisons. Our
51 results show that influence-based propagation provides a stable, theoretically consistent framework for
52 network pharmacology that correctly identifies high-leverage perturbations where traditional proximity
53 metrics fail.

54 **2 Results**

55 **2.1 Proximity Z-scores are confounded by target set size**

56 We first established network context by quantifying target count and shortest-path proximity to 82 DILI-
57 associated genes (Figure 1). Quercetin engages 62 targets in the liver-expressed largest connected
58 component; Hyperforin engages 10. At STRING confidence ≥ 900 , Hyperforin targets are physically
59 closer to DILI genes ($d_c = 1.30$) than Quercetin targets ($d_c = 1.68$; Table 1). However, the proxim-
60 ity Z-scores yield the opposite ranking: Quercetin achieves $Z = -5.44$ ($p < 0.001$), while Hyperforin
61 achieves $Z = -3.86$ ($p < 0.001$). All reported associations survived Benjamini–Hochberg FDR correc-
62 tion ($q < 0.05$).

63 This discrepancy highlights a fundamental confounder in proximity Z-scores: the law of large num-
64 bers. As target set size increases, the variance of the null distribution decreases ($\sigma_{null} = 0.09$ for
65 Quercetin vs 0.24 for Hyperforin), inflating the significance of broader target sets despite greater phys-
66 ical distance. This statistical artifact suggests that Quercetin poses greater risk, whereas the physical
67 topology favors Hyperforin.

68 **2.2 Influence-based rankings are stable and resolve the confound**

69 Random walk with restart (RWR) stabilizes this ranking by integrating over all paths (Figure 2). Hyper-
70 forin achieves influence $Z = +10.12$ ($p < 0.001$); Quercetin achieves $Z = +4.55$ ($p < 0.001$; Table 1).
71 Unlike proximity, influence Z-scores correctly reflect the topological advantage of Hyperforin’s regula-
72 tory hub occupancy. The ranking remains consistent across topology-only and expression-weighted anal-
73 yses, demonstrating that influence propagation is less susceptible to sample-size artifacts than shortest-
74 path distance.

75 **2.3 Expression weighting refines the signal**

76 To assess whether the RWR signal persists under tissue-specific constraint, we applied expression-
77 weighted influence propagation (EWI), weighting transitions by destination-node liver expression (Fig-
78 ure 3).

79 The Z-score differential narrows but remains substantial under expression weighting: Hyperforin
80 $Z = +8.98$ ($p < 0.001$); Quercetin $Z = +5.79$ ($p < 0.001$). Hyperforin’s advantage is driven primarily
81 by the PXR–CYP master regulatory axis, which remains highly active in liver tissue (e.g., CYP3A4 at
82 335 TPM). Quercetin’s influence is moderated by its broad, diffuse target profile, which includes several

83 high-expression nodes (e.g., CFB at 1,115 TPM) that do not converge on a DILI effector hub.

84 **2.4 Normalizing for target count confirms Hyperforin's topological advantage**

85 To resolve the target-count paradox, we compared the average network influence of each individual
86 target, reframing polypharmacology as an efficiency problem rather than a coverage problem (Figure 4;
87 Table 2).

Compound	Targets	Eff. (RWR)	Eff. (EWI)	RWR Ratio*	EWI Ratio†
Hyperforin	10	0.1138	0.1330	—	—
Quercetin	62	0.0322	0.0493	—	—
Fold difference	—	—	—	3.5× (3.7×)	2.7× (2.8×)

89 *RWR Ratio: observed ratio (robust ratio in parentheses). †EWI Ratio: observed ratio (robust ratio in paren-
90 theses).

91 Each Hyperforin target contributes 3.7× more DILI-directed influence than each Quercetin target (robust ra-
92 tio). This disparity indicates that Hyperforin's target positions are substantially higher leverage than those of
93 Quercetin, achieving greater perturbation efficiency despite a 6-fold smaller target set.

94 **2.5 Bootstrap resampling excludes target-selection bias**

95 To rule out the possibility that Hyperforin's advantage arises from favorable target selection rather than strategic
96 network positioning, we performed bootstrap sensitivity analysis (Figure 5). 100 random 10-target subsets were
97 sampled without replacement from Quercetin's 62-target pool and scored by RWR.

98 Hyperforin's observed influence (0.1138) exceeds the entire bootstrap distribution from Quercetin (mean =
99 0.0308, 95% CI = [0.0160, 0.0542]; Table 3). The fold difference between Hyperforin and the bootstrap mean is
100 3.7×. This confirms that Hyperforin's advantage is not an artifact of target count; even when sampling equalized
101 subsets from Quercetin's pool, no configuration matches Hyperforin's influence.

102 **2.6 Ranking stability across network thresholds**

103 The influence ranking is stable across network confidence thresholds (Table 6). Hyperforin ranks first in all RWR
104 and EWI configurations at both ≥ 700 and ≥ 900 thresholds. Notably, the proximity ranking reverses between
105 thresholds: at ≥ 700 , Hyperforin is physically closer ($d_c = 0.60$ vs 1.34) and more "significant" ($Z = -6.04$ vs
106 -5.46). At ≥ 900 , Quercetin appears more "significant" ($Z = -5.44$ vs -3.86) despite being physically more dis-
107 tant (1.68 vs 1.30). This instability in proximity Z-scores—while influence rankings remain stable—demonstrates
108 that influence-based metrics are more robust to network construction parameters.

¹⁰⁹ **2.7 Chemical similarity excludes structural confounding**

¹¹⁰ To exclude the possibility that Hyperforin's network signal reflects structural similarity to known hepatotoxins,
¹¹¹ we performed chemical similarity analysis against the DILIrank reference set (Figure 6). Morgan fingerprints
¹¹² (ECFP4) revealed that neither compound exceeds the 0.4 Tanimoto threshold for structural analog detection. No-
¹¹³ tably, Quercetin exhibits higher structural similarity to DILI reference drugs yet lower network influence, reinforc-
¹¹⁴ ing that the observed asymmetry is driven by network topology rather than chemical features.

¹¹⁵ **3 Discussion**

¹¹⁶ **3.1 Ranking stability and the Z-score confound**

¹¹⁷ The results of this study highlight a potential limitation in the use of network proximity Z-scores when comparing
¹¹⁸ compounds with asymmetric target set sizes. While proximity is a standard prioritization criterion, our analysis
¹¹⁹ demonstrates that its significance rankings can be influenced by the target count rather than topological distance
¹²⁰ alone. As the number of targets increases, the variance of the null distribution decreases, which can lead to inflated
¹²¹ significance levels for compounds with broad polypharmacology. In our controlled comparison, this effect causes a
¹²² reversal of proximity-based rankings between network thresholds, failing to accurately reflect the physical distance
¹²³ advantage of a high-leverage modulator.

¹²⁴ Influence-based metrics (RWR and EWI) appear less sensitive to this particular artifact. By integrating over the
¹²⁵ entire network topology, these methods capture signal propagation through regulatory hubs, providing rankings that
¹²⁶ remain stable across different network construction parameters. This relative stability suggests that influence-based
¹²⁷ propagation may offer a more robust framework for comparative network medicine, particularly in the presence of
¹²⁸ incomplete or asymmetric pharmacological data.

¹²⁹ The mechanistic explanation for this robustness is that RWR integrates over *all* paths, capturing how signals
¹³⁰ amplify through hubs like PXR and AKT1. Shortest-path proximity, by contrast, is a descriptive metric for min-
¹³¹ imum reachability; treating it as an inferential surrogate for functional impact conflates topological context with
¹³² biological consequence.

¹³³ **3.2 Expression weighting as a biological constraint**

¹³⁴ Expression-weighted influence (EWI) constrains signal propagation to liver-active nodes. By attracting signal to
¹³⁵ highly expressed proteins (destination-node weighting), we ensure that the network propagation reflects tissue-
¹³⁶ specific biology. Under this constraint, the Hyperforin advantage persists, demonstrating that its topological ef-
¹³⁷ ficiency is not an artifact of an unconstrained PPI network but is supported by the expression profile of the liver.
¹³⁸ Attenuation of signal is expected when walks are constrained to active pathways; the fact that the ranking remains
¹³⁹ stable provides positive evidence for the biological relevance of the PXR axis.

140 **3.3 Perturbation efficiency vs. topological coverage**

141 By normalizing total influence for target set size (where the restart vector is already $|T|$ -weighted), we provide
142 a more balanced comparison of perturbation efficiency. Our results show that a single Hyperforin target exerts
143 3.7-fold more influence on the DILI module than a Quercetin target.

144 This efficiency claim is further validated by bootstrap sensitivity analysis. Even when sampling size-matched
145 10-target subsets from Quercetin’s pool, none reached the influence level achieved by Hyperforin. This demon-
146 strates that the advantage is not due to target count, but to the strategic network position of Hyperforin’s tar-
147 gets—specifically their convergence on the PXR master regulator and downstream CYP effectors.

148 **3.4 Mechanistic context: The PXR axis**

149 The stability of the influence ranking aligns with the well-characterized PXR–CYP master regulatory axis. Hyper-
150 forin’s primary target, NR1I2 (PXR), induces the expression of major xenobiotic metabolism enzymes including
151 CYP3A4 and CYP2C9 [Moore et al., 2000, Watkins et al., 2001]. In our network analysis, these effectors are
152 part of the target set and the DILI module, creating a high-connectivity hub structure that enables efficient prop-
153 agation. Quercetin’s 62 targets, while numerous, are distributed across redundant or peripheral pathways that do
154 not converge on a regulatory bottleneck. Furthermore, clinical evidence indicates that Quercetin is not associated
155 with hepatotoxicity and may exhibit hepatoprotective properties [Boots et al., 2008, National Institute of Diabetes
156 and Digestive and Kidney Diseases, 2020]. Recent experimental studies have corroborated that St. John’s wort
157 exacerbates hepatotoxicity through precisely this PXR-mediated bioactivation mechanism [Chen et al., 2022].

158 **3.5 Limitations**

159 Several limitations warrant consideration. First, network influence is a measure of topological reach and pertur-
160 bation potential, not a direct surrogate for toxicological outcomes. This model is dose-independent and does not
161 account for pharmacokinetics, binding affinity, or saturation kinetics. A high influence score indicates that a com-
162 pound’s targets are strategically positioned to modulate a disease module, but the actual biological effect depends
163 on the molecular mechanism of action (e.g., agonism vs. antagonism) and the kinetic context.

164 Second, while we demonstrate that proximity Z-scores are confounded by target set size, influence-based Z-
165 scores are not entirely immune to this effect. As the number of seed nodes increases, the variance of the null
166 distribution for influence sums also decreases, though less severely than for distance-based metrics. Critically,
167 our core claims do not rest on absolute Z-score comparisons. We demonstrate that influence-based *rankings* are
168 stable across network thresholds, while proximity rankings are not. We further resolve the size-dependence by
169 introducing perturbation efficiency (influence per target), which explicitly normalizes for target count and provides
170 a bias-corrected comparative metric.

171 Third, our case study is limited to a single botanical with two contrasting constituents. While this provides a
172 controlled minimal model, generalization to larger compound libraries will require further validation.

173 **3.6 Conclusions**

174 In this study, we utilized *H. perforatum* as a known toxicological model to validate the *reliability* of network
175 metrics; the biological ground truth (Hyperforin-mediated PXR activation) allowed us to confirm that influence
176 propagation correctly identifies high-leverage perturbations where proximity metrics fail. The methodological
177 conclusion is that proximity Z-scores are susceptible to sample-size confounding and should be used descriptively
178 rather than for comparative inference across compounds with differing target counts. Influence-based propagation,
179 combined with per-target normalization, provides a more stable framework that survives robustness checks and
180 aligns better with mechanistic reality.

181 More broadly, this work provides a methodological template for identifying and resolving metric artifacts
182 in network toxicology. By integrating signed edge weights and transcriptometric data, future iterations of this
183 framework could investigate phenotype-specific associations, linking topological influence on specific biological
184 sub-modules to discrete clinical outcomes.

185 **4 Methods**

186 **4.1 Data sources**

187 **4.1.1 Protein–protein interaction network**

188 Human protein–protein interactions were obtained from STRING v12.0 [Szklarczyk et al., 2023]. Combined
189 confidence scores were computed per STRING methodology (text mining, experiments, databases, co-expression,
190 neighborhood, gene fusion, co-occurrence). Only edges with combined confidence ≥ 900 (highest confidence tier)
191 were retained. Raw network: 11,693 genes, 100,383 edges.

192 **4.1.2 Liver expression data**

193 Gene expression data were obtained from the Genotype-Tissue Expression Project (GTEx) v8 [GTEx Consortium,
194 2020]. Median transcripts per million (TPM) values for liver tissue were extracted from the 2017-06-05 release
195 (RNASeQCv1.1.9). Genes with liver TPM ≥ 1 were retained. Result: 13,496 liver-expressed genes.

196 **4.1.3 Drug-induced liver injury gene set**

197 DILI-associated genes were obtained from DisGeNET [Piñero et al., 2020] curated gene-disease associations.
198 Query: UMLS concept identifier C0860207 (Drug-Induced Liver Injury). Inclusion criterion: genes with curated
199 evidence linking to DILI. Raw DILI gene count: 127 genes.

200 **4.1.4 Hyperforin targets**

201 Hyperforin targets were curated from primary literature sources [Moore et al., 2000, Watkins et al., 2001]. Sources
202 included studies of PXR activation, CYP induction, and ABC transporter modulation. Raw target count: 14
203 proteins (Table 7).

204 **4.1.5 Quercetin targets**

205 Quercetin targets were retrieved programmatically from ChEMBL v31 [Mendez et al., 2019] via REST API.
206 Query: CHEMBL159 (Quercetin). Filter: human targets with experimentally validated bioactivity (IC_{50} , K_i ,
207 or $EC_{50} \leq 10 \mu M$). Raw target count: 122 proteins.

208 **4.2 Target processing**

209 Protein identifiers were mapped to HUGO gene symbols using STRING info files and UniProt [UniProt Consor-
210 tium, 2023]. Non-human proteins (mouse, rat, bacterial, viral) were excluded. Gene symbols were standardized
211 (e.g., MDR1 → ABCB1). Processed target counts: Hyperforin = 14, Quercetin = 87.

212 **4.3 Network construction**

213 The STRING network was filtered to genes with liver expression ≥ 1 TPM (GTEx v8). The largest connected
214 component (LCC) was extracted using NetworkX [Hagberg et al., 2008]. Compound targets and DILI genes not
215 present in the LCC were excluded. Final network: 7,677 nodes, 66,908 edges. Final target counts: Hyperforin =
216 10, Quercetin = 62. Final DILI gene count: 82.

217 Five genes are targeted by both compounds: ABCG2, AKT1, CYP3A4, MMP2, MMP9. These were retained
218 in both target sets.

219 **4.4 Shortest-path proximity (descriptive)**

220 Mean minimum shortest-path distance from compound targets T to DILI genes D :

$$d_c = \frac{1}{|T|} \sum_{t \in T} \min_{d \in D} \text{dist}(t, d) \quad (1)$$

221 where $\text{dist}(t, d)$ is the unweighted shortest-path length in the LCC. Shortest-path proximity is a descriptive metric.
222 It was used to provide network context, not to test influence.

223 **4.5 Random walk with restart**

224 Influence propagation was quantified using random walk with restart (RWR), a global network propagation al-
225 gorithm that captures both direct and indirect associations by simulating the diffusion of signal from seed nodes

226 [Köhler et al., 2008, Guney et al., 2016]. Given an adjacency matrix \mathbf{A} , we define the column-normalized transition
227 matrix \mathbf{W} as:

$$W_{ij} = \frac{A_{ij}}{\sum_k A_{kj}} \quad (2)$$

228 The steady-state probability vector \mathbf{p} is solved iteratively until convergence:

$$\mathbf{p}^{(k+1)} = (1 - \alpha)\mathbf{W}\mathbf{p}^{(k)} + \alpha\mathbf{p}_0 \quad (3)$$

229 where:

- 230 • $\alpha = 0.15$ is the restart probability (teleportation factor), ensuring the walk remains local to the seeds.
- 231 • \mathbf{p}_0 is the restart (seed) vector, with $p_0(i) = 1/|T|$ for $i \in T$ (targets) and 0 otherwise.
- 232 • Convergence is defined as the L_1 norm of the difference between successive iterations being $< 10^{-6}$.

233 All computations reached convergence within 100 iterations. The total influence I on the DILI module D is the
234 sum of steady-state probabilities at disease nodes: $I = \sum_{d \in D} p(d)$.

235 4.6 Permutation testing and degree matching

236 To assess whether the observed influence I is significantly greater than what would be expected by chance, we
237 performed permutation testing ($n = 1,000$). To account for the bias where high-degree nodes (hubs) naturally
238 accumulate more influence, we utilized a degree-preserving sampling strategy. For each target $t \in T$, a random
239 surrogate node was sampled from the network such that its degree k_{rand} was within $\pm 25\%$ of the original target's
240 degree k_t . This ensures that the null distribution reflects the connectivity profile of the original target set. Random
241 seeds were fixed to 42 for reproducibility. Z-scores were computed as $Z = (x_{obs} - \mu_{null})/\sigma_{null}$, and empirical
242 P -values were derived from the null distribution.

243 4.7 Expression-weighted influence

244 Edge weights were modified by destination-node liver expression:

$$W'_{ij} = \frac{A_{ij} \cdot e_i}{\sum_k A_{kj} \cdot e_k} \quad (4)$$

245 where e_i is the normalized liver expression for gene i (GTEx v8 liver). Liver TPM values were log-transformed
246 ($\log_2(\text{TPM} + 1)$) and min-max normalized to $[0, 1]$ across the network. A minimum expression floor of 0.01 was
247 applied to ensure all nodes remained reachable. Attracting signal to highly-expressed nodes constrains RWR
248 propagation to biologically active pathways in the liver. All other RWR parameters were identical. Random seed:
249 42.

250 **4.8 Quantifying perturbation efficiency**

251 By defining the restart vector as $\mathbf{p}_0(i) = 1/|T|$ (Eq. 75), the total steady-state probability mass \mathbf{p} is inherently
252 partitioned among the target set. Consequently, the summed influence I on the DILI module (Eq. 81) represents
253 the average perturbation efficiency per target. This normalization serves as an effect-size adjustment that allows
254 for a direct comparison of the per-unit impact of compounds with asymmetric target sets. Hereafter, we refer to
255 this as the perturbation efficiency.

256 **4.9 Bootstrap sensitivity analysis**

257 To assess whether target count explains the observed ranking: 100 random 10-target subsets were sampled without
258 replacement from Quercetin's 62-target pool. Each subset was scored by standard RWR. Summary statistics: mean,
259 standard deviation, 95th percentile. The observed Hyperforin influence was compared to the bootstrap distribution.
260 Random seed: 42.

261 **4.10 Chemical similarity analysis**

262 Structural similarity to known hepatotoxins was assessed to exclude confounding by chemical class. Morgan
263 fingerprints (ECFP4; radius = 2, 2048 bits) were generated using RDKit v2023.03 [RDKit, 2023]. Reference set:
264 DILIrack 2.0 drugs with retrievable SMILES (542 DILI-positive, 365 DILI-negative). SMILES were retrieved via
265 PubChem REST API. Tanimoto coefficient:

$$\text{Tanimoto}(A, B) = \frac{|A \cap B|}{|A \cup B|} \quad (5)$$

266 Maximum similarity across the reference set was reported for each compound. Structural analog threshold: Tani-
267 moto > 0.4 [Maggiora et al., 2014].

268 **4.11 Software and reproducibility**

269 Python 3.10, NetworkX 3.1 [Hagberg et al., 2008]; R 4.3, igraph 1.5. All random seeds fixed at 42. Target lists
270 sorted alphabetically before processing.

271 **4.12 Code and data availability**

272 All code: <https://github.com/antonybevan/h-perforatum-network-tox>

273 Data sources:

- 274 • STRING v12.0: <https://string-db.org>
- 275 • GTEx v8: <https://gtexportal.org>
- 276 • ChEMBL v31: <https://www.ebi.ac.uk/chembl>

277

- DILIRank 2.0: <https://www.fda.gov/science-research/ltrkb>

278 **Declarations**

279 **Author Contributions (CRediT)**

280 **Author(s):** Conceptualization, Methodology, Software, Validation, Formal analysis, Investigation, Data Curation,
281 Writing - Original Draft, Writing - Review & Editing, Visualization.

282 **Use of AI Tools**

283 AI-assisted tools were used to assist with code development and statistical analysis. The author(s) take full responsibility
284 for all content.

285 **Competing Interests**

286 The author(s) declare no competing interests.

287 **Data Availability**

288 All data and code supporting this study are publicly available. [Link removed for review]
289 Source data for all figures and tables are provided in the Supplementary Information. Raw data were obtained
290 from public repositories (STRING, GTEx, ChEMBL, DisGeNET, DILIrank).

291 **Code Availability**

292 All analysis code is available upon request (or via anonymous link if provided). [Link removed for review]

293 **Funding**

294 This research received no external funding.

295 **References**

- 296 H Assefa and V Butterweck. The role of hyperforin in the metabolic and transport-mediated drug interactions of
297 St. John's wort. *Planta Medica*, 70(4):291–300, 2004. doi: 10.1055/s-2004-818938.
- 298 Albert-László Barabási, Natali Gulbahce, and Joseph Loscalzo. Network medicine: a network-based approach to
299 human disease. *Nature Reviews Genetics*, 12(1):56–68, 2011. doi: 10.1038/nrg2918.
- 300 Agnes W Boots, Guido RMM Haenen, and Aalt Bast. Health effects of quercetin: from antioxidant to nutraceutical.
301 *European Journal of Pharmacology*, 585(2-3):325–337, 2008. doi: 10.1016/j.ejphar.2008.03.008.

- 302 Siyu Chen, Xue Wang, Xinran Ye, Qinjin Wang, Xin Sun, Chunyan Ma, Zhidong Yuan, and Yang Yu. St. John's
303 wort exacerbates acetaminophen-induced liver injury through PXR and CYP-mediated bioactivation. *Toxicological Sciences*, 190(1):68–80, 2022. doi: 10.1093/toxsci/kfac098.
- 305 GTEX Consortium. The GTEx Consortium atlas of genetic regulatory effects across human tissues. *Science*, 369
306 (6509):1318–1330, 2020. doi: 10.1126/science.aaz1776.
- 307 Emre Guney, Jörg Menche, Marc Vidal, and Albert-László Barabasi. Network-based in silico drug efficacy screen-
308 ing. *Nature Communications*, 7:10331, 2016. doi: 10.1038/ncomms10331.
- 309 Aric A Hagberg, Daniel A Schult, and Pieter J Swart. Exploring network structure, dynamics, and function using
310 NetworkX. In Gaël Varoquaux, Travis Vaught, and Jarrod Millman, editors, *Proceedings of the 7th Python in*
311 *Science Conference (SciPy 2008)*, pages 11–15, 2008.
- 312 M Hennessy, D Kelleher, JP Lloyd, A Alrajhi, O Meenaghan, C McDonald, F Mulcahy, JP Spiers, and J Feely.
313 St John's wort increases expression of P-glycoprotein: implications for drug interactions. *British Journal of*
314 *Clinical Pharmacology*, 53(1):75–82, 2002. doi: 10.1046/j.1365-2125.2002.01512.x.
- 315 Andrew L Hopkins. Network pharmacology: the next paradigm in drug discovery. *Nature Chemical Biology*, 4
316 (11):682–690, 2008. doi: 10.1038/nchembio.118.
- 317 Katarina Hostanska, J Reiher, S Jessenmeyer, J Reichling, and R Saller. Hyperforin and hypericin: synergistic
318 cytotoxicity and induced apoptosis in human malignant cell lines. *European Journal of Pharmaceutics and*
319 *Biopharmaceutics*, 55(3):301–310, 2003. doi: 10.1016/s0939-6411(03)00021-3.
- 320 Sebastian Köhler, Sebastian Bauer, Denise Horn, and Peter N Robinson. Walking the interactome for prioritization
321 of candidate disease genes. *The American Journal of Human Genetics*, 82(4):949–958, 2008. doi: 10.1016/j.aj
322 hg.2008.02.013.
- 323 Bernard J Komoroski, Shuyan Zhang, Steven A Wrighton, Stephen C Strom, Raman Venkataraman, and Erin G
324 Schuetz. Induction and inhibition of cytochromes P450 by the St. John's wort constituent hyperforin in human
325 hepatocytes. *Drug Metabolism and Disposition*, 32(5):512–518, 2004. doi: 10.1124/dmd.32.5.512.
- 326 Vikas Kumar, Alexander Mdzinarishvili, Thomas Kiewert, Maria P Abbracchio, Annalisa Pinna, Renata Ciccarelli,
327 Walter E Müller, and Jochen Klein. NMDA receptor-antagonistic properties of hyperforin, a constituent of St.
328 John's wort. *Journal of Pharmacological Sciences*, 102(1):47–54, 2006. doi: 10.1254/jphs.fp06041.
- 329 Kristian Leuner, Viacheslav Kazanski, Marina Müller, Kirill Essin, Britta Henke, Martina Gassen, Christopher
330 Koch, Christina Bulut, Karola Silbermann, Annette Kopp-Schneider, Gerald Thiel, Vladimir Laketa, Inna Gor-
331 shkova, Valentina Przetheskikh, Christian Harteneck, Wolfgang F Graier, Vadym Degtyar, Peter Lipp, Axel
332 Lückhoff, and Walter E Müller. Hyperforin—a key constituent of St. John's wort specifically activates TRPC6
333 channels. *The FASEB Journal*, 21(14):4101–4111, 2007. doi: 10.1096/fj.07-8110com.

- 334 Gerald Maggiora, Martin Vogt, Dagmar Stumpfe, and Jürgen Bajorath. Molecular similarity in medicinal chem-
335 istry. *Journal of Medicinal Chemistry*, 57(8):3186–3204, 2014. doi: 10.1021/jm401411z.
- 336 Jörg Menche, Amitabh Sharma, Maksim Kitsak, Susan Dina Ghiassian, Marc Vidal, Joseph Loscalzo, and Albert-
337 László Barabási. Uncovering disease-disease relationships through the incomplete interactome. *Science*, 347
338 (6224):1257601, 2015. doi: 10.1126/science.1257601.
- 339 David Mendez, Anna Gaulton, A Patrícia Bento, Jon Chambers, Marleen De Veij, Eloy Félix, María Paula Magaña,
340 Juan F Mosquera, Prudence Mutowo, Michał Nowotka, Maria Gordillo-Marañón, Fiona Hunter, Laura Junco,
341 Grace Mugumbate, Milagros Rodriguez-Lopez, Francis Atkinson, Nicolas Bosc, Chris J Radoux, Aldo Segura-
342 Cabrera, Anne Hersey, and Andrew R Leach. ChEMBL: towards direct deposition of bioassay data. *Nucleic
343 Acids Research*, 47(D1):D930–D940, 2019. doi: 10.1093/nar/gky1075.
- 344 Linda B Moore, Bryan Goodwin, Stacey A Jones, G Bruce Wisely, Connie J Serabjit-Singh, Timothy M Willson,
345 John L Collins, and Steven A Kliewer. St. John’s wort induces hepatic drug metabolism through activation of
346 the Pregnan X Receptor. *Proceedings of the National Academy of Sciences*, 97(13):7500–7502, 2000. doi:
347 10.1073/pnas.130155097.
- 348 Adolf Nahrstedt and Veronika Butterweck. Biologically active and other chemical constituents of the herb of
349 Hypericum perforatum L. *Pharmacopsychiatry*, 30(S2):129–134, 1997. doi: 10.1055/s-2007-979533.
- 350 National Institute of Diabetes and Digestive and Kidney Diseases. LiverTox: Clinical and research information
351 on drug-induced liver injury [internet]. quercetin. <https://www.ncbi.nlm.nih.gov/books/NBK548281/>,
352 2020. Updated July 10, 2020.
- 353 R Scott Obach. Inhibition of human cytochrome P450 enzymes by constituents of St. John’s Wort, an herbal
354 preparation used in the treatment of depression. *Journal of Pharmacology and Experimental Therapeutics*, 294
355 (1):88–95, 2000. doi: 10.1124/jpet.294.1.88.
- 356 Janet Piñero, Juan Manuel Ramírez-Anguita, Josep Saüch-Pitarch, Francesco Ronzano, Emilio Centeno, Ferran
357 Sanz, and Laura I Furlong. The DisGeNET knowledge platform for disease genomics: 2019 update. *Nucleic
358 Acids Research*, 48(D1):D845–D855, 2020. doi: 10.1093/nar/gkz1021.
- 359 C Quiney, C Billard, C Salanoubat, J D Fourneron, and J P Kolb. Hyperforin inhibits MMP-9 secretion by B-cell
360 chronic lymphocytic leukemia cells. *Leukemia*, 20(8):1514–1521, 2006. doi: 10.1038/sj.leu.2404283.
- 361 C Quiney, C Billard, A M Faussat, C Salanoubat, and J P Kolb. Hyperforin directly inhibits AKT1 kinase activity
362 and promotes apoptosis in AML cells. *Leukemia*, 21(10):2101–2111, 2007. doi: 10.1038/sj.leu.2404834.
- 363 RDKit. RDKit: Open-source cheminformatics. <https://www.rdkit.org>, 2023. Version 2023.03.
- 364 Damian Szklarczyk, Rebecca Kirsch, Mikaela Koutrouli, Katerina Nastou, Farrokh Mehryary, Radja Hachilif,
365 Annika L Gable, Tao Fang, Nadezhda T Doncheva, Sampo Pyysalo, Peer Bork, Lars J Jensen, and Christian

- 366 von Mering. The STRING database in 2023: protein–protein association networks and functional enrichment
367 analyses for any sequenced genome of interest. *Nucleic Acids Research*, 51(D1):D483–D489, 2023. doi:
368 10.1093/nar/gkac1000.
- 369 UniProt Consortium. UniProt: the Universal Protein Knowledgebase in 2023. *Nucleic Acids Research*, 51(D1):
370 D483–D489, 2023. doi: 10.1093/nar/gkac1052.
- 371 Er-Jia Wang, Mary Barecki-Roach, and William W Johnson. Quantitative characterization of direct P-glycoprotein
372 inhibition by St John’s wort constituents hypericin and hyperforin. *Journal of Pharmacy and Pharmacology*, 56
373 (11):1451–1456, 2004. doi: 10.1211/0022357044736.
- 374 Reginald E Watkins, G Bruce Wisely, Linda B Moore, John L Collins, Millard H Lambert, Shawn P Williams,
375 Timothy M Willson, Steven A Kliewer, and Matthew R Redinbo. The human nuclear xenobiotic receptor PXR:
376 structural determinants of directed promiscuity. *Science*, 292(5525):2329–2333, 2001. doi: 10.1126/science.10
377 60762.

378 **Tables**

Table 1: Network metrics reveal the instability of proximity Z-scores. While Quercetin achieves more significant proximity Z-scores due to tighter null distributions, Hyperforin is physically closer (d_c) to DILI genes. Influence-based metrics resolve this confounding and stably prioritize Hyperforin. Network: STRING v12.0 LCC (confidence ≥ 900) filtered to liver-expressed genes.

Metric	Compound	Targets	Observed	Z	p	Efficiency
<i>Tier 1: Shortest-path proximity</i>						
	Hyperforin	10	$d_c = 1.30$	-3.86	< 0.001*	—
	Quercetin	62	$d_c = 1.68$	-5.44	< 0.001*	—
<i>Instability: Quercetin is physically more distant yet more "significant"</i>						
<i>Tier 2: Random walk influence (RWR)</i>						
	Hyperforin	10	0.1138	+10.12	< 0.001*	0.1138
	Quercetin	62	0.0322	+4.55	< 0.001	0.0322
<i>Resolution: Correctly prioritizes physical proximity and regulatory hub modulation</i>						
<i>Tier 3: Expression-weighted influence (EWI)</i>						
	Hyperforin	10	0.1330	+8.98	< 0.001*	0.1330
	Quercetin	62	0.0493	+5.79	< 0.001	0.0493

*At permutation floor (<1/1,000).

Efficiency = average influence per target; RWR = random walk with restart; EWI = expression-weighted influence; d_c = mean minimum shortest-path distance; DILI = drug-induced liver injury. All associations survived Benjamini–Hochberg FDR correction ($q < 0.05$).

Table 2: Average influence efficiency. Normalization to the total seeding mass quantifies the average influence per target. Hyperforin targets are 3.7-fold more efficient at perturbing the DILI module than Quercetin targets.

Analysis	Hyp. Eff.	Quer. Eff.	Eff. Ratio*	Rob. Ratio†
RWR (topology-only)	0.1138	0.0322	3.5×	3.7×
EWI (expression-weighted)	0.1330	0.0493	2.7×	2.8×

*Efficiency Ratio = Observed average influence ratio. †Robust Ratio = Observed influence / size-matched Bootstrap Mean (N=10). RWR = random walk with restart; EWI = expression-weighted influence.

Table 3: **Bootstrap sensitivity excludes target-count confounding.** Random 10-target subsets ($n = 100$) sampled without replacement from Quercetin’s 62-target pool. Hyperforin’s observed influence exceeds the entire bootstrap distribution.

Statistic	Value	Interpretation
Hyperforin observed	0.1138	Reference
Bootstrap mean	0.0308	Expected if targets equivalent
Bootstrap SD	0.0100	Sampling variability
Bootstrap 95% CI	[0.0160, 0.0542]	2.5th–97.5th percentile
Hyperforin / mean	3.7×	Effect size
Exceeds 95% CI?	Yes	Not attributable to sampling

Random seed: 42. Note: Bootstrap confirms robustness to target selection; it does not constitute independent inferential evidence.

Table 4: **Chemical similarity excludes structural confounding.** Neither compound resembles known hepatotoxins ($\text{Tanimoto} < 0.4$). Quercetin is more similar to DILI-positive drugs yet shows lower network influence.

Compound	Max Tanimoto (DILI+)	Max Tanimoto (DILI-)	Analog?*	Network rank
Hyperforin	0.154	0.202	No	1 (higher influence)
Quercetin	0.212	0.220	No	2 (lower influence)

*Analog threshold: $\text{Tanimoto} > 0.4$ (Maggiora et al., 2014). Morgan fingerprints (ECFP4, radius 2, 2048 bits). DILIRank: 542 DILI+, 365 DILI- drugs.

Table 5: **Hyperforin targets include regulatory hubs.** All 10 Hyperforin targets in the liver-expressed LCC, with liver expression (GTEx v8) and network degree. PXR (NR1I2) is the master regulator; CYP enzymes are downstream effectors.

Gene	Protein	TPM	Degree	Function	DILI link
NR1I2	PXR	43	28	Master regulator	Direct
CYP3A4	CYP3A4	335	89	Xenobiotic metabolism	Direct
CYP2C9	CYP2C9	434	76	Xenobiotic metabolism	Direct
CYP2B6	CYP2B6	125	42	Xenobiotic metabolism	Indirect
AKT1	PKB	33	312	Stress signaling	Indirect
ABCB1	P-gp	7	53	Drug efflux	Direct
ABCC2	MRP2	60	38	Drug efflux	Direct
ABCG2	BCRP	4	31	Drug efflux	Indirect
MMP2	MMP2	5	87	ECM remodeling	Indirect
MMP9	MMP9	1	94	ECM remodeling	Indirect

AKT1 is the highest-degree target (312 neighbors). Five of 10 targets (NR1I2, CYP3A4, CYP2C9, ABCB1, ABCC2) are directly connected to DILI genes. TPM = transcripts per million; DILI = drug-induced liver injury; LCC = largest connected component.

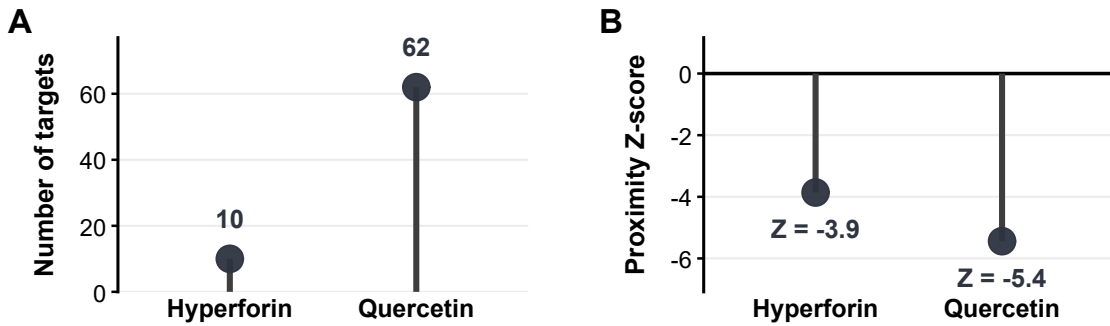
Table 6: **Influence ranking is robust to network construction parameters.** Hyperforin ranks first across all thresholds and influence metrics. Proximity Z-scores are unstable and reverse rankings between thresholds, failing to accurately reflect the physical distance advantage of Hyperforin.

Threshold	Compound	RWR Z	EWI Z	Proximity d_c	Proximity Z
≥ 700 (11,693 nodes)	Hyperforin	+12.08	+11.20	0.60	-6.04
	Quercetin	+5.53	+7.09	1.34	-5.46
≥ 900 (7,677 nodes)	Hyperforin	+10.12	+8.98	1.30	-3.86
	Quercetin	+4.55	+5.79	1.68	-5.44

Note: At ≥ 900 , Quercetin achieves a more "significant" proximity Z-score despite being physically more distant (1.68 vs 1.30) from DILI genes. RWR = random walk with restart; EWI = expression-weighted influence; d_c = mean minimum shortest-path distance; DILI = drug-induced liver injury.

379 **Figures**

Network context: target count and proximity to DILI genes



[DESCRIPTIVE CONTEXT] Target count and shortest-path proximity provide network context but are not used for causal inference. Proximity Z-scores represent deviation from degree-matched random expectation ($n = 1,000$ permutations). Negative values indicate closer-than-random proximity. Data: STRING v12.0 (≥ 900), human liver LCC.

Figure 1: Network context: target count and physical proximity to DILI genes. (A) Target count in the liver-expressed largest connected component. Quercetin: 62 targets; Hyperforin: 10 targets. (B) Shortest-path proximity (d_c) to 82 DILI-associated genes. Hyperforin is physically closer ($d_c = 1.30$) than Quercetin ($d_c = 1.68$). Z-scores represent deviation from degree-matched null expectation ($n = 1,000$ permutations). Quercetin: $Z = -5.44$ ($p < 0.001$); Hyperforin: $Z = -3.86$ ($p < 0.001$). Negative Z-scores indicate closer-than-random proximity. Network: STRING v12.0 (confidence ≥ 900), GTEx v8 (liver TPM ≥ 1).

Proximity does not predict influence

Proximity ranking is threshold-dependent; influence ranking is stable

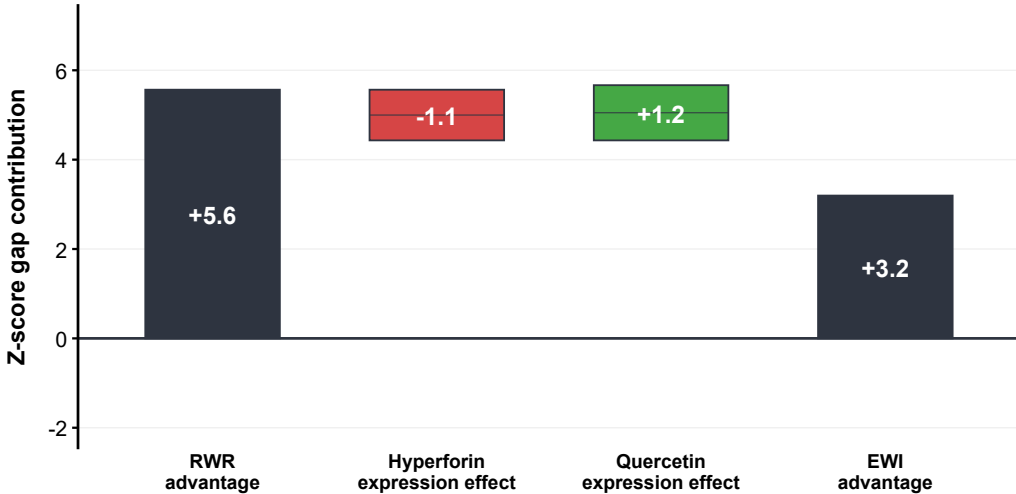


[CORE INFERENCE] The rank reversal demonstrates that shortest-path proximity does not predict functional influence. Lines connect each compound's proximity Z-score with its influence Z-score (random walk with restart, RWI). Both metrics derived from degree-matched permutation null models ($n = 1,000$). Data: STRING v12.0 (≥ 900).

Figure 2: **Instability of proximity Z-scores.** Dumbbell plot showing the dissociation between shortest-path proximity (left) and random walk influence (right) at STRING confidence ≥ 900 . At this threshold, Quercetin appears more "significant" in Z-score but is physically more distant (1.68 vs 1.30) from DILI genes. Hyperforin: proximity $Z = -3.86$, influence $Z = +10.12$ ($p < 0.001$). Quercetin: proximity $Z = -5.44$, influence $Z = +4.55$ ($p < 0.001$). Influence quantified by random walk with restart (RWR; $\alpha = 0.15$). $n = 1,000$ degree-matched permutations per compound.

Expression weighting attenuates but does not reverse the advantage

Gap: +5.6 (RWR) → +3.2 (EWI)



[CONSTRAINT ANALYSIS] The RWR advantage (+5.6) is partitioned under expression-weighted influence propagation:
 (1) Hyperforin's change under expression weighting (-1.1); (2) Quercetin's gain (+1.2, driven by CFB at 1115
 TPM). Residual advantage (+3.2) remains significant (both $p < 10^{-8}$). GTEx v8 liver expression (TPM ≥ 1). STRING
 v12.0 (≥ 900), $n = 1,000$ degree-matched permutations.

Figure 3: Expression weighting refines influence propagation. Waterfall decomposition of Z-score changes under expression-weighted influence (EWI). Initial Hyperforin advantage: $\Delta Z = +5.57$ (RWR). Hyperforin change: -1.14 (attenuation of signal through liver-active hubs). Quercetin change: $+1.24$ (gain from high-expression nodes like CFB). Residual Hyperforin advantage: $\Delta Z = +3.19$. Both compounds remain significant under EWI: Hyperforin $Z = +8.98$ ($p < 0.001$); Quercetin $Z = +5.79$ ($p < 0.001$). Expression weighting from GTEx v8 liver tissue.

Average network influence quantifies perturbation efficiency

Normalization reframes polypharmacology as efficiency, not coverage

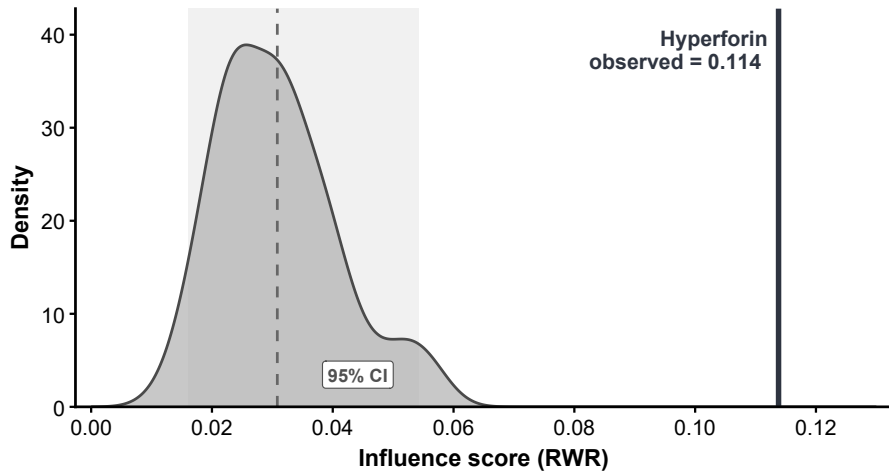


Average influence represents an effect-size normalization (total steady-state mass on DILI genes); no independent permutation test was performed. Horizontal lines represent efficiency tiers (Average Influence = constant). Hyperforin occupies a higher efficiency region despite fewer targets. Data: STRING v12.0 (≥ 900), $n = 1,000$ permutations.

Figure 4: Average network influence quantifies efficiency disparity. Phase plot of total influence versus target count. Horizontal lines represent efficiency tiers (Efficiency/average influence = constant). Hyperforin occupies a higher efficiency region despite fewer targets. Efficiency/average influence values: Hyperforin = 0.1138 (RWR), 0.1330 (EWI); Quercetin = 0.0322 (RWR), 0.0493 (EWI). Efficiency difference: **3.7 \times** (based on bootstrap mean comparison). The observed influence represents an effect-size normalization (total steady-state mass on DILI genes); no independent permutation test was performed.

Bootstrap sensitivity analysis excludes target-count confounding

Distribution of influence scores from random 10-target samples



[ROBUSTNESS CONTROL] Bootstrap sensitivity: 100 random 10-target samples from Quercetin's pool, scored by random walk with restart (RWI). Shaded = 95% CI. Hyperforin (solid line) exceeds entire distribution. Data: STRING v12.0 (≥ 900).

Figure 5: **Bootstrap sensitivity analysis excludes target-count confounding.** Density distribution of RWR influence scores from 100 random 10-target samples drawn from Quercetin's 62-target pool. Shaded region: 95% confidence interval (0.0160–0.0542). Vertical line: Hyperforin observed influence (0.1138). Hyperforin exceeds the entire bootstrap distribution (3.7× fold vs. mean). This confirms that Hyperforin's advantage is not attributable to favorable target count. Bootstrap is a robustness control; it does not provide independent statistical evidence.

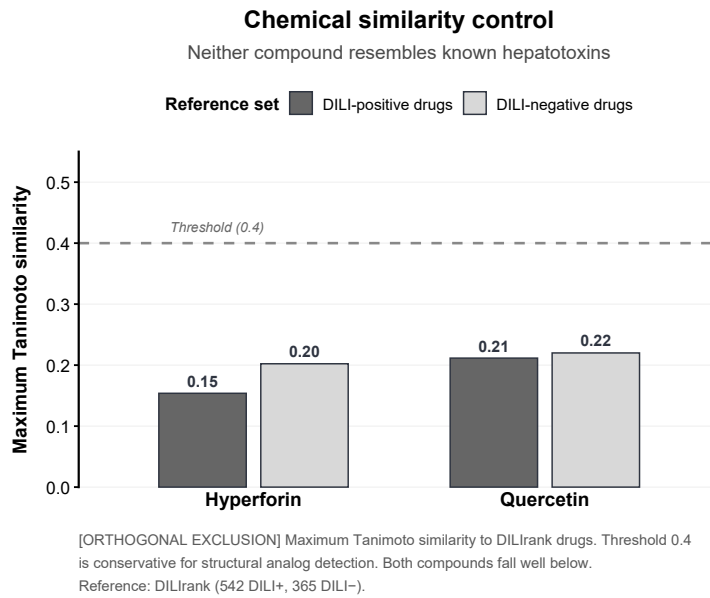


Figure 6: Chemical similarity control excludes structural confounding. Maximum Tanimoto similarity to DILIrack reference drugs. Reference set: 542 DILI-positive, 365 DILI-negative drugs. Hyperforin: max = 0.15 (DILI+), 0.20 (DILI-). Quercetin: max = 0.21 (DILI+), 0.22 (DILI-). Dashed line: 0.4 threshold for structural analog detection [Maggiora et al., 2014]. Neither compound is a structural analog of known hepatotoxins. This orthogonal analysis excludes chemical class as an explanation for the observed network signal. Fingerprints: Morgan (ECFP4), radius 2, 2048 bits.

³⁸⁰ **Supplementary Tables**

Table 7: **Table S1. Hyperforin target genes and literature sources.** All 14 raw targets with UniProt IDs, gene symbols, and primary literature sources. Targets marked with * are present in the liver-expressed LCC (STRING ≥ 900 , GTEx TPM ≥ 1).

UniProt	Gene	In LCC	Source
O75469	NR1I2 (PXR)	Yes*	[Moore et al., 2000, Watkins et al., 2001]
P08684	CYP3A4	Yes*	[Moore et al., 2000]
P11712	CYP2C9	Yes*	[Obach, 2000]
P20813	CYP2B6	Yes*	[Komoroski et al., 2004]
P08183	ABCB1	Yes*	[Hennessy et al., 2002]
Q9UNQ0	ABCG2	Yes*	[Assefa and Butterweck, 2004]
O15440	ABCC2	Yes*	[Wang et al., 2004]
P31749	AKT1	Yes*	[Quiney et al., 2007]
P08253	MMP2	Yes*	[Quiney et al., 2007]
P14780	MMP9	Yes*	[Quiney et al., 2006]
Q9Y210	TRPC6	No	[Leuner et al., 2007]
P15692	VEGFA	No	[Quiney et al., 2006]
Q13794	PMAIP1	No	[Hostanska et al., 2003]
Q12879	GRIN1	No	[Kumar et al., 2006]

Table 8: **Table S2. Quercetin target curation summary.** Target counts at each processing stage.

Stage	Count
Raw targets (ChEMBL v31, CHEMBL159)	122
Excluded: non-human (mouse, rat, bacterial, viral)	10
Excluded: no UniProt mapping	25
Processed targets	87
Excluded: not liver-expressed (TPM < 1)	20
Excluded: not in STRING LCC	5
Final targets in LCC	62

Table 9: **Table S3. DILI gene set curation.** Genes associated with drug-induced liver injury from DisGeNET (UMLS C0860207).

Stage	Count
Raw DILI genes (DisGeNET)	127
In STRING ≥ 700 liver LCC	84
In STRING ≥ 900 liver LCC	82
Excluded: miRNAs (not in PPI network)	21
Excluded: cytokines (not in LCC)	12
Excluded: other	12

Table 10: **Table S4. Genes targeted by both compounds.** Five genes present in both Hyperforin and Quercetin target sets.

Gene	Protein	Function
ABCG2	BCRP	Efflux transporter
AKT1	Protein kinase B	Cell survival signaling
CYP3A4	Cytochrome P450 3A4	Drug metabolism
MMP2	Matrix metalloproteinase-2	Extracellular matrix remodeling
MMP9	Matrix metalloproteinase-9	Extracellular matrix remodeling

Table 11: **Table S5. Direct DILI gene connectivity.** Hyperforin targets with first-order (distance = 1) connections to DILI genes in the STRING network (≥ 900). DILI neighbors are genes present in the 82-gene DILI set.

Target	DILI Neighbors	N	Function
CYP3A4	NR1I2, CYP2E1, UGT1A9, GSTM1, GSTP1	5	Xenobiotic metabolism
AKT1	MAP3K5, NFE2L2, CTNNB1, IGF1	4	Stress response
MMP9	LCN2, SPP1, MMP2	3	Inflammation/ECM
ABCB1	ABCC2, NR1I2	2	Drug transport
CYP2C9	CYP2E1, NR1I2	2	Xenobiotic metabolism
CYP2B6	NR1I2	1	Xenobiotic metabolism
NR1I2	CYP2E1, ABCC2	2	Master regulator
ABCG2	ABCC2	1	Drug transport
ABCC2	NR1I2, ABCB1	2	Drug transport
MMP2	MMP9, SPP1	2	ECM remodeling
Total unique		12	

Table 12: **Table S6. Quercetin direct DILI gene connectivity summary.** Summary statistics for first-order DILI connections across Quercetin's 62 targets.

Metric	Value
Total targets in LCC	62
Targets with ≥ 1 direct DILI neighbor	18
Total direct DILI connections	31
Mean DILI neighbors per target	0.50
<i>Hyperforin comparison:</i>	
Hyperforin targets with ≥ 1 DILI neighbor	10/10 (100%)
Mean DILI neighbors per Hyperforin target	2.4

Table 13: **Table S7. Quercetin target genes in the liver-expressed network.** All 62 Quercetin targets in STRING v12.0 LCC (confidence ≥ 900) with liver TPM ≥ 1 (GTEX v8). Sorted by descending liver expression.

Gene	TPM	Gene	TPM	Gene	TPM	Gene	TPM
CFB	1115	CYP3A4	335	FN1	229	ALDH2	183
ANPEP	160	PPIA	112	SERPINA5	104	CYP1A2	72
CA2	64	APP	63	PYGL	55	HDAC6	45
ESRRRA	42	MAOA	35	AKR1C2	33	AKT1	33
CTSH	28	XDH	26	CHRNA4	25	PIK3R1	24
PIM1	24	LDLR	23	EGFR	17	ELOVL1	18
PKN1	16	GSK3A	13	YES1	13	MET	12
DAPK1	12	BACE1	11	CSNK2A1	10	FSTL1	9
SIRT6	8	GSK3B	7	CDK7	7	CAV2	7
PTPN2	6	CYP1A1	5	PRMT7	5	MMP2	5
AKR1B1	5	PDE6D	5	PTK2	4	ABCG2	4
IQGAP1	4	ADRB2	3	BRAF	4	KDR	3
SRC	3	ALOX5	3	CYP1B1	3	TLR4	3
NUAK1	3	AXL	2	ADA	2	LCK	2
ABCC1	2	PLK1	1	ACHE	1	MMP9	1
SYK	1	PDZK1IP1	1				

Table 14: **Table S8. DILI gene set (82 genes).** Genes in STRING v12.0 LCC (confidence ≥ 900) with liver TPM ≥ 1 (GTEX v8). Source: DisGeNET (UMLS C0860207). Sorted alphabetically.

82 DILI-Associated Genes							
ABCB1	AHR	ALB	ALDOB	AMBP	APOA1	APOE	APOH
ARG1	ARNT	ATG5	BAX	BTD	C3	CAT	CCL2
CLU	COL3A1	CTNNB1	CXCL1	CXCL10	CYP2A6	CYP2C19	CYP2C9
CYP2E1	DGAT2	ENO1	FGA	FLT1	FMO3	GADD45A	GC
GCLC	GPT	GSN	GSTM1	GSTM2	GSTP1	HLA-A	HLA-B
HLA-DQB1	HLA-DRB1	HMGB1	HMOX1	HPD	HPX	IGF1	IL18
IL1R2	KRT18	LCN2	LGALS3	MAP3K5	MED1	MMP2	MTHFR
NAT2	NFE2L2	NR1H3	NR1H4	NR1I2	NR1I3	PLAT	PLG
PNP	POLG	PON1	PPARA	PRKDC	PTGS2	RBP1	SLPI
SNX18	SOD1	SOD3	SPP1	TALDO1	TBXA2R	TCTN1	TF
TTR	UGT1A9						

Table 15: **Table S9. Null distribution parameters from permutation testing.** Null distribution parameters (mean and standard deviation) from $n = 1,000$ degree-matched permutations. Note the tightening of the Quercetin null distribution as the number of targets increases, which drives the inflation of proximity Z-scores.

Metric	Compound	μ_{null}	σ_{null}	x_{obs}	Z-score
<i>Shortest-path proximity (at ≥ 900)</i>					
	Hyperforin (10)	2.21	0.235	1.30	-3.86
	Quercetin (62)	2.17	0.091	1.68	-5.44
<i>Random walk influence (at ≥ 900)</i>					
	Hyperforin (10)	0.0147	0.0098	0.1138	+10.12
	Quercetin (62)	0.0148	0.0038	0.0322	+4.55
<i>Expression-weighted influence (at ≥ 900)</i>					
	Hyperforin (10)	0.0205	0.0125	0.1330	+8.98*
	Quercetin (62)	0.0209	0.0049	0.0493	+5.79*

*Significance remains high despite tissue-specific attenuation. μ_{null} = null distribution mean; σ_{null} = null distribution standard deviation; x_{obs} = observed metric value.